Malsur Dharavath
DRDL, DRDO,
Hyderabad, Andhra Pradesh 500058, India
e-mail: malsurd@gmail.com

P. Manna
DRDL, DRDO,
Hyderabad, Andhra Pradesh 500058, India
e-mail: pbmanna999@gmail.com

P. K. Sinha
DRDL, DRDO,
Hyderabad, Andhra Pradesh 500058, India
e-mail: pksinha@drdl.drdo.in

Debasis Chakraborty[1]
DRDL, DRDO,
Hyderabad, Andhra Pradesh 500058, India
e-mail: debasis_cfd@drdl.drdo.in

Numerical Analysis of a Kerosene-Fueled Scramjet Combustor

A kerosene-fueled scramjet combustor was numerically analyzed in order to meet the requirement of thrust for a hypersonic test vehicle. The internal configuration of the fuel injection struts and fuel injection was arrived through computational fluid dynamics (CFD) study. The combustor was tested in the hypersonic test facility at DRDL. Numerical simulations were carried out along with facility nozzle (from throat onward) both for nonreacting and reacting flow. Three-dimensional (3D) Reynolds-averaged Navier–Stokes (RANS) equations are solved along with k–ε turbulence model. Single-step chemical reaction with Lagrangian particle tracking method (LPTM) is used for combustion of kerosene fuel. Fairly good match of the top wall pressure has been obtained with experimental data for both nonreacting and reacting flows. Effects of mass flow rate of incoming vitiated air and fuel flow have been studied numerically in details. Top wall pressure distributions have been found to decrease with the decrease of the mass flow rate of vitiated air. Significant drop of wall pressure, higher thrust per unit fuel flow, and combustion efficiency have been observed with the decrease of fuel flow. [DOI: 10.1115/1.4030699]

1 Introduction

Air-breathing engines are considered to be one of the preferred propulsion devices for atmospheric flight. Combustion should take place at supersonic speed when the flight Mach number is hypersonic ($M > 5$). Supersonic combustion ramjet (scramjet) is the key enabling technology for transatmospheric-sustained flights in hypersonic speed. In scramjet engines, the combustor length is typically of the order of 1–1.5 m and the residence time of the fuel–air mixture is of the order of a millisecond (for flight Mach numbers from 6 to 8). Generation of useful thrust over the vehicle drag through heat addition at such high speeds is challenging, owing to the fact that the fuel has to mix and burn completely within the combustor length. Research and development of an efficient hypersonic air-breathing vehicle powered by scramjet engine was started in the early 1960s [1–3]. Both hydrogen and kerosene were studied extensively. Hydrogen-fueled scramjet engine was considered for space applications, whereas hydrocarbon fuel was considered for air-launched missiles leading toward the development of hypersonic vehicle with scramjet engine. Though, hydrogen is attractive because of having higher specific impulse and better ignition characteristics, liquid hydrocarbon was preferred for its higher density and easier handling issue in hypersonic military applications ($M < 8$). However, the liquid fuel has to atomize and evaporate before mixing and combustion with the mainstream air which adds an additional time delay for the heat release and thus necessitating a longer residence time and, in turn, a longer combustor length. Design of the internal configuration for fuel injection is crucial for proper mixing of fuel with air, ignition, and combustion, and to provide the required thrust within the specified length of the combustor. Since the mixing and combustion of fuel with air occur at supersonic speed, scramjet researchers always face big challenges in respect of proper mixing of fuel with air, ignition, and combustion inside the combustor. Mixing of fuel with incoming supersonic air stream is a challenging issue for hydrocarbon combustion. A deeper penetration of fuel [4] into a supersonic air stream is required for better mixing which is a key to sustained combustion. The typical penetration depth of the fuel jet is about 10–15 mm for a practical scramjet combustor in the flight region of Mach 6.0–7.0. Reported experimental and numerical studies [5–7] on hydrocarbon fueled supersonic combustion mostly address the issues of cavity-based flame holder and injection system in laboratory scaled combustor. The penetration of liquid fuel in supersonic flow is critical in any practical scramjet combustor. The problem of slow lateral fuel transport in the air stream can be circumvented by injecting the fuel in the core region of the flow by means of struts and/or pylons. The oblique shocks generated from the struts also augment the mixing which is very much needed in high-speed propulsion devices.

The studies on strut-based scramjet combustor with kerosene fuel are highly limited. Fuel injection from the struts has been experimented upon in some subscale scramjet engine including airframe integrated scramjet module [8,9]. The subscale strut-based scramjet engine being developed at NAL (Kakuda, Japan) [9] uses the fuel injection strut to improve mixing.

With the advent of powerful computer and robust numerical algorithm, CFD is playing an important role in developing a comprehensive understanding of the key phenomenon that dominates performances. To accurately model scramjet flow field, CFD must adequately resolve several complex physical processes including three-dimesionality, shock boundary interaction, turbulent mixing of high-speed streams, atomization, and combustion of liquid fuel. Only few numerical studies were reported on strut-based liquid-fueled scramjet combustor. Dufour and Bouchez [10] have numerically simulated the scramjet experiment [11] using a 3D Navier–Stokes solver and single-step chemical kinetics. A reasonably good match is obtained between the computational and experimentally measured wall static pressure. Montgomery et al. [12] have implemented reduced chemical kinetic mechanisms for combustion of various hydrocarbon fuels into the VULCAN CFD code and used for simulations of a 3D scramjet flameholder. Manna et al. [13] numerically explored the effect of the combustor inlet Mach number and total pressure on the flow development in the scramjet combustor. It has been shown that higher combustor entry, Mach number, and distributed fuel injection are required to obtain predominant supersonic flow and avoid thermal choking.

[1]Corresponding author.

Contributed by the Heat Transfer Division of ASME for publication in the Journal of Thermal Science and Engineering Applications. Manuscript received April 15, 2014; final manuscript received January 26, 2015; published online November 11, 2015. Assoc. Editor: Suman Chakraborty.

A hypersonic air-breathing cruise vehicle with airframe integrated scramjet engine was presented by Pannerselvam et al. [14]. One-dimensional flow model was developed for the design and performance prediction of various individual components, such as forebody, intake, combustor, and nozzle.

In this work, 3D viscous simulations are presented for a full scale flight module scramjet combustor for hypersonic air-breathing mission with kerosene fuel injected from a row of struts placed in the flow path. Combustor entry conditions have been taken corresponding to the equivalent flight condition of the hypersonic air-breathing cruise vehicle [14]. Thermochemical parameters are analyzed to estimate the flow behavior inside the combustor. The effects of air mass flow and fuel flow rate on combustion efficiency and performance are presented.

2 Solution Methodology

Commercial CFD software CFX-11 [15] is used for the present analysis. CFX is a fully implicit 3D RANS code, capable of solving diverse and complex turbulent reacting fluid flow problems. The code is a fully implicit, finite volume method with FE-based discretization of geometry. The method retains much of the geometric flexibility of finite element methods as well as the important conservation properties of the finite volume method. It utilizes numerical upwind schemes to ensure global convergence of mass, momentum, energy, and species. It implements a general nonorthogonal, structured, boundary fitted grids. To circumvent the initial numerical transient, the discretization of the convective terms is done by first-order upwind difference scheme till few time steps initially and subsequently, the convective terms are discretized through second-order scheme to capture the flow features more accurately. Turbulence was modeled using k–ε model. Wall functions were used to model flow near the walls.

For combustion, the eddy dissipation model (EDM) is used for its simplicity and robustness in predicting the performance of reactive flows in many engineering applications. The EDM is based on the concept that chemical reaction is fast compared to the transport process in the flow. When reactants mix at the molecular level, they instantaneously form products. The model assumes that the reaction rate may be related directly to the time required to mix reactants at molecular level. In turbulent flows, this mixing time is dictated by the eddy properties and therefore, the burning rate is in proportional to the rate at which turbulent kinetic energy is dissipated, i.e., reaction rate is proportional to ε/k, where k is the turbulent kinetic energy and ε is its rate of dissipation. The chemistry of the kerosene ($C_{12}H_{23}$) reaction is represented on a molar basis by

$$C_{12}H_{23} + 17.75O_2 = 12CO_2 + 11.5H_2O$$

The mixing rate determined from the EDM is given as

$$R_{k,EDM} = -A_{ebu}\rho\frac{\varepsilon}{k}\min\left\{y_f, \frac{y_{ox}}{r_k}, B_{ebu}\frac{y_p}{1+r_k}\right\}$$

where ρ and y_f, y_{ox}, and y_p are the density and mass fractions of fuel, oxidizer, and products, respectively, A_{ebu} and B_{ebu} are the model constants, and r_k is the stoichiometric ratio.

LPTM is used for discrete phase model to characterize the flow behavior of the dispersed phase fluid (kerosene liquid) along with the flow of the continuous phase predicted using a discretized form of the RANS equations. Solutions are marched with global time step typically at 10^{-5} s. Log-normalized maximum residue of -04 is considered as the convergence criteria.

The software (CFX) is thoroughly validated for the reported literature for hydrogen and hydrocarbon fuels injected from wall, cavity, pylon, and struts, and the simulation results were published in Refs. [16–19].

3 Combustor Configuration and Inflow Details

Hot air for the test is generated by burning small amount of hydrogen with incoming air in a heater which gives rise to high pressure and temperature of the test air in the heater. The vitiated air (contains superheated water vapor) was passed through a convergent and divergent nozzle to give the required conditions for the scramjet. The combustor geometry with eight strut arrangement along with the divergent facility nozzle is shown in Fig. 1.

The length of the divergent portion of the facility nozzle is $2.9h$ with a $0.37h$ constant area included at the exit in order to settle the flow before the entry to the combustor. Where h is the height of the combustor at the inlet as shown in Fig. 1. The width of the combustor is $6.4h$. The cross sections of the nozzle at throat and exit are $6.4h \times 0.56h$ and $6.4h \times 1.0h$, respectively. The length of the combustor is $21.5h$. An additional length of $1.2h$ constant area is added at the end of the combustor to provide support to the combustor. The cross sections at the entry and exit of the combustor are $6.4h \times 1.0h$ and $6.4h \times 2.93h$, respectively. The combustor has a constant area section of $1.05h$ from entry of the combustor, followed by 1 deg divergent section of $2.3h$, 4 deg divergent section for $7.33h$, and finally a 7.5 deg divergent section of $9.9h$ length. A middle wall of $0.14h$ thickness has been attached at $X = 2.9h$ at the middle of the combustor which makes combustor into two modules, named as, left module (LM) and right module (RM). Four struts are provided in each module in a similar manner from the middle wall (as shown in Fig. 1), first strut being near to the middle wall and fourth strut near to the side wall. The location of the first, second, third, and fourth struts is $3.72h$, $5.17h$, $6.92h$, and $8.84h$ from the combustor inlet in the X-axis whereas $0.49h$, $1.27h$, $2.03h$, and $2.81h$ from the middle of the combustor in the width, respectively.

The schematic of typical strut geometry is shown in Fig. 2. The cross section from the leading edge is sweeping backward in the upper and lower parts. Marquardt Corporation (Cazenovia, NY) [20] has investigated this sweptback type of strut in scramjet combustor to increase the three dimensionality of the flow. Leading edges with small radius and blunt trailing edges have been provided in the strut to keep the shock attached and for flame holding purpose, respectively. Detailed computational studies were carried out to find out the number of struts for fuel injection, their configuration and injection locations as a part of the development of hypersonic vehicle program [14]. The cross-sectional length and the base width of the struts are $0.51h$ and $0.13h$, respectively. In the simulation, X-axis is taken along the length of combustor, while Y- and Z-axis are chosen along the height and width of the combustor, respectively, with the origin being placed at the middle of the bottom wall at combustor inlet.

Liquid kerosene fuel is injected through 208 injection points provided in eight struts. Each strut contains 13 injection holes on either side. All the injection holes are approximately of the same size having a diameter of 0.5 mm. Full geometry was taken for the simulation as there were slight differences (approximately few

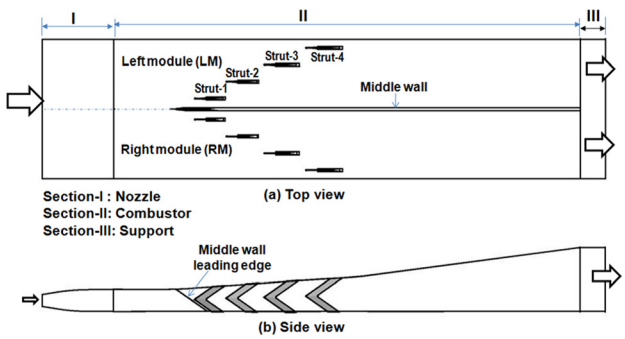

Fig. 1 Details of the scramjet combustor: (*a*) top view and (*b*) side view

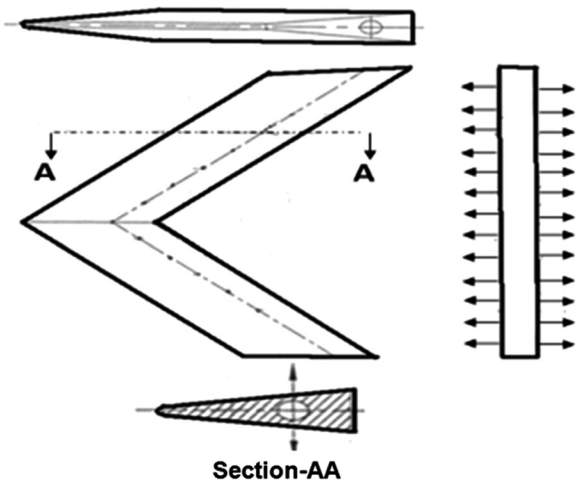

Fig. 2 Typical strut geometry

millimeter) between the two modules (LM and RM) in the manufactured combustor. The simulations were carried out both for nonreacting and reacting flow. Additionally, to see the effect of leakage of kerosene which was observed during the test; two more simulations have been carried out by reducing the fuel equivalence ratio to (1) 10% and (2) 20%. A Rosin–Rammler particle distribution of diameter $D = 37.32\,\mu$m and dispersion factor of $\gamma = 1.5$ has been considered for all the reacting flow simulations. An equivalence ratio of 1.0 is considered for reacting flow simulations.

4 Results and Discussion

4.1 Computational Grid. Block-structured grids are made using ICEM CFD [21] for the entire domain. A total $316 \times 55 \times 175$ ($\sim 3 \times 10^6$) number of structured grids are used in the simulations. The typical grid distributions in *X–Y*, *X–Z*, and *Y–Z* plane are shown in Figs. 3(*a*)–3(*c*), respectively. The grids are fine near the leading edge and trailing regions of the struts, adjoining region between the nozzle and combustor, and near wall regions, while relatively coarser grids are provided in the remaining portion of the combustor.

4.2 Boundary Conditions. All the flow properties are kept constant at the inflow plane, as the inflow boundary is supersonic. No slip and adiabatic wall boundary conditions are imposed at the walls. The ambient pressure outflow boundary condition has been imposed at the exit of the combustor as the combustor is tested at ambient condition. When the combustor is analyzed to calculate the thrust availability, simulations have been carried out with supersonic outflow boundary condition at the exit of the computational domain. Log-normalized maximum residue of −04 is considered as convergence criteria.

4.3 Nonreacting Flow Simulation Results. The qualitative features of the nonreacting flow field have been presented through the Mach number, static pressure (P/P_s, P_s being the static pressure at combustor entry), and static temperature (T/T_s, T_s being the static temperature at combustor entry) distribution in different planes ($X = -3.3h$ (nozzle entry), 0.0 (combustor entry), $2.9h$, $5.8h$, $8.7h$, $11.6h$, $14.5h$, $17.4h$, and $21.5h$ (combustor exit)) in Fig. 4. Flow is found to expand in the divergent nozzle. Mach number value of 1.89 has been achieved at the entry of the combustor. Flow in the combustor is largely supersonic in the combustor upto about $X = 12.0h$, after which the separation of the flow has been found toward the exit of the combustor due to the presence of ambient pressure (outflow) condition. Flow in the combustor after $12h$ becomes subsonic because of the presence of terminal shock through which the combustor pressure rises to atmospheric pressure. Static pressure and temperature have been found to decrease upto the middle ($X = 1.0$) of the combustor due to the expansion in the divergent combustor, but increases afterward due to the equalization of pressure with the ambient condition at the outlet of the combustor. Top wall pressure comparison between the experimental and CFD at $Z = 1.6h$ is shown in Fig. 5 for both for LM and RM. Fairly good match has been obtained between the two results. The measured nozzle exit wall pressure P_s matches exactly with CFD simulation result.

4.4 Reacting Flow Simulation. Reacting flow simulations are carried out with transverse injection of liquid kerosene fuel into the supersonic air (vitiated) flow through the four struts in each module. Based on the mass flow rate of vitiated air, mass fraction of O_2 available in the vitiated air, and the injected kerosene flow, the equivalence ratios are calculated to be almost unity for all the cases. The thermochemical flow parameters are described by the distribution of Mach number, pressure, temperature, and mass fractions of carbon dioxide (CO_2), oxygen (O_2), kerosene vapor ($C_{12}H_{23}$), whereas quantitative comparisons are made for top wall pressure, average Mach number, static pressure and temperature, combustion efficiency, thrust, etc.

4.4.1 Reacting Flow Simulation Result (Baseline). Mach number, static pressure, and static temperature distribution at different axial stations ($X = -3.3h$ (nozzle entry), 0.0 (combustor entry), $2.9h$, $5.8h$, $8.7h$, $11.6h$, $14.5h$, $17.4h$, and $21.5h$ (combustor exit)) are shown in Figs. 6(*a*)–6(*c*), respectively, whereas the average values of the same along the length of the combustor are shown in Figs. 7(*a*)–7(*c*), respectively.

Due to reaction of the fuel, Mach number values come down, static pressure and temperature increase in the middle of the

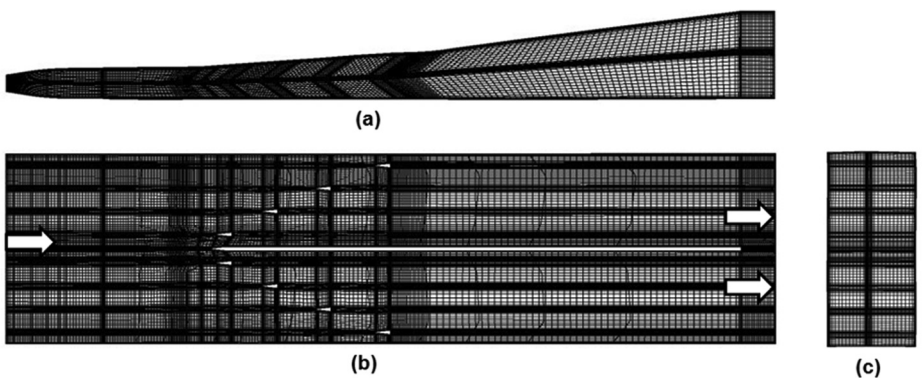

Fig. 3 Grid distribution at different planes of the scramjet combustor: (*a*) *X–Y* plane, (*b*) *X–Z* plane, and (*c*) *Y–Z* plane

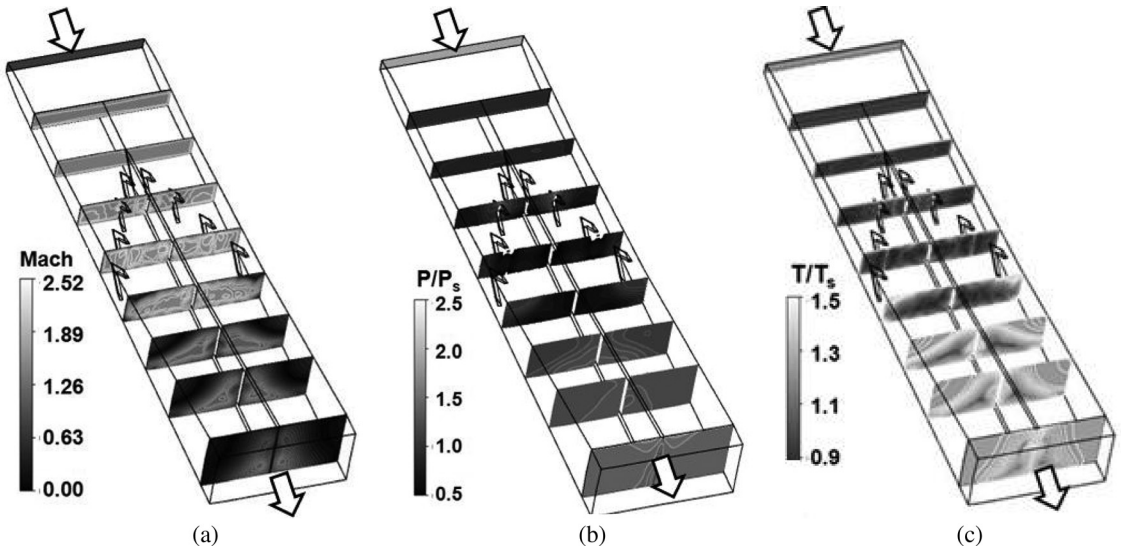

Fig. 4 (*a*) Mach number, (*b*) static pressure, and (*c*) static temperature distribution at various axial planes

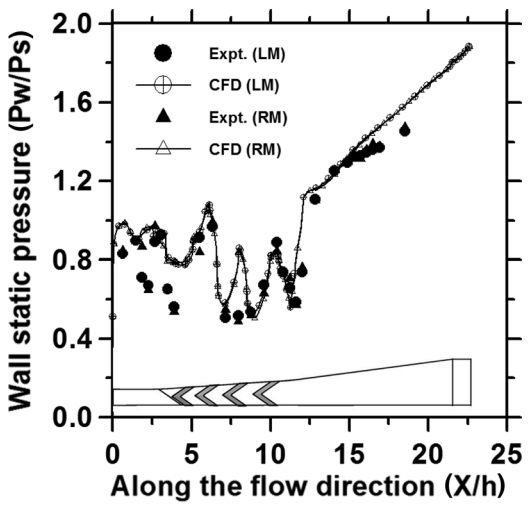

Fig. 5 Comparison of nonreacting top wall pressure distribution ($Z = 1.6h$)

combustor, adjacent to the strut regions. Average Mach number has been found below unity at $X = 4.9h$–$10.8h$. Flow is not fully subsonic in the range. There are some subsonic pockets (caused due to reaction) in the downstream of the struts. These subsonic pockets are responsible to bring the average Mach number below unity. Afterward, the flow starts expanding at 7.5 deg divergent section of the combustor causing Mach number to increase and static pressure and temperature to decrease. Toward the exit of the combustor, flow is compressed due to the influence of ambient pressure (which is higher than the expanding flow pressure) causing Mach number to decrease and static pressure and temperature to rise. The average Mach number has been found to become subsonic again at $X = 17.0h$ and continued to be subsonic upto the exit of the combustor.

Mass fraction of CO_2, O_2, and $C_{12}H_{23}$ at various axial locations is shown in Figs. 8(*a*)–8(*c*), respectively. Reaction pattern for both the modules (LM and RM) looks almost similar. Liquid kerosene droplets completely vaporize within the combustor and no liquid droplets are found at the exit of the combustor. However, some of the unburnt kerosene is observed adjacent to the middle wall regions. Combustion efficiency is defined as the ratio of the

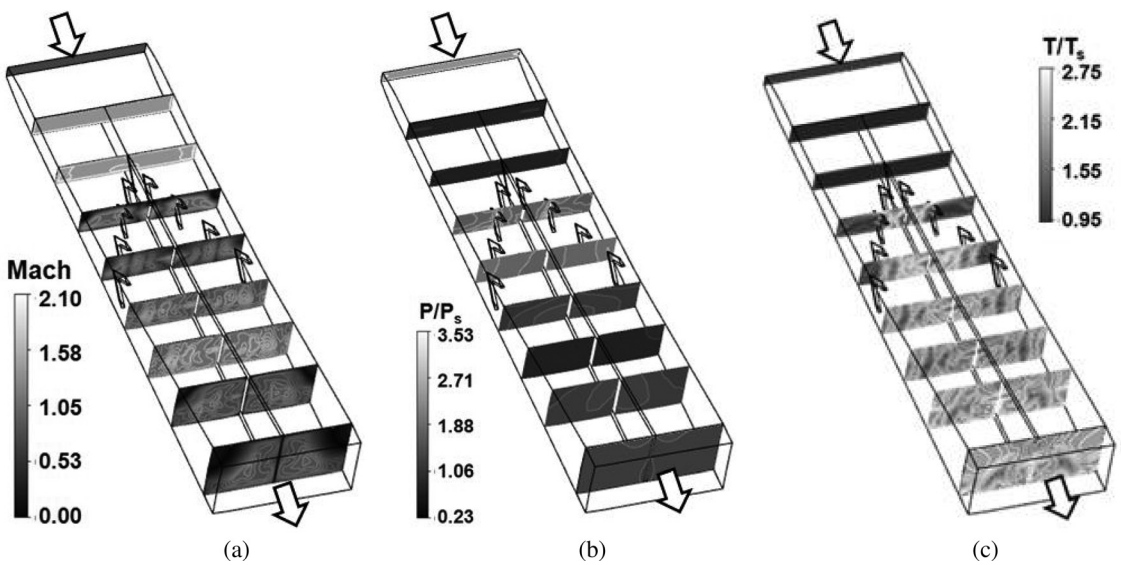

Fig. 6 (*a*) Mach number, (*b*) static pressure, and (*c*) static temperature distribution for reacting flows at various axial planes

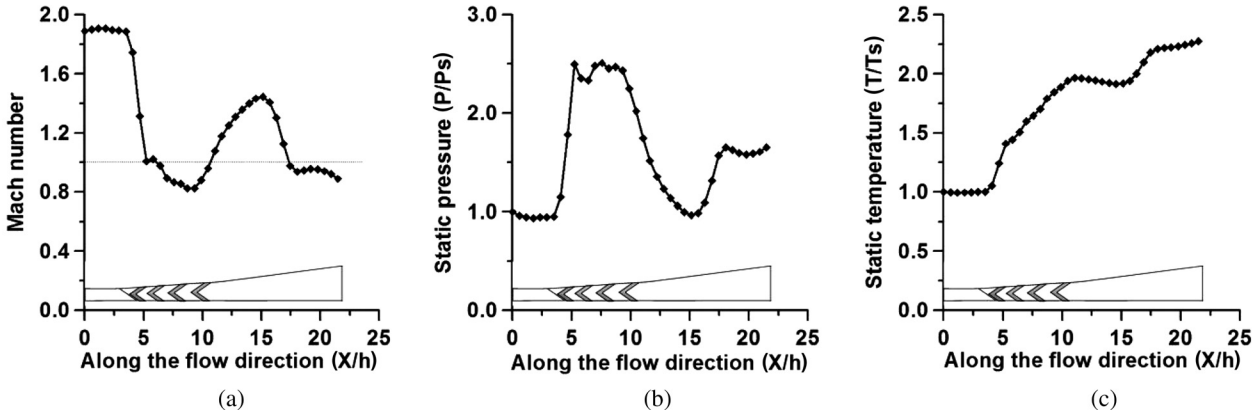

Fig. 7 Average Mach number (*a*), static pressure (*b*), and static temperature (*c*) distribution for reacting flows along the length

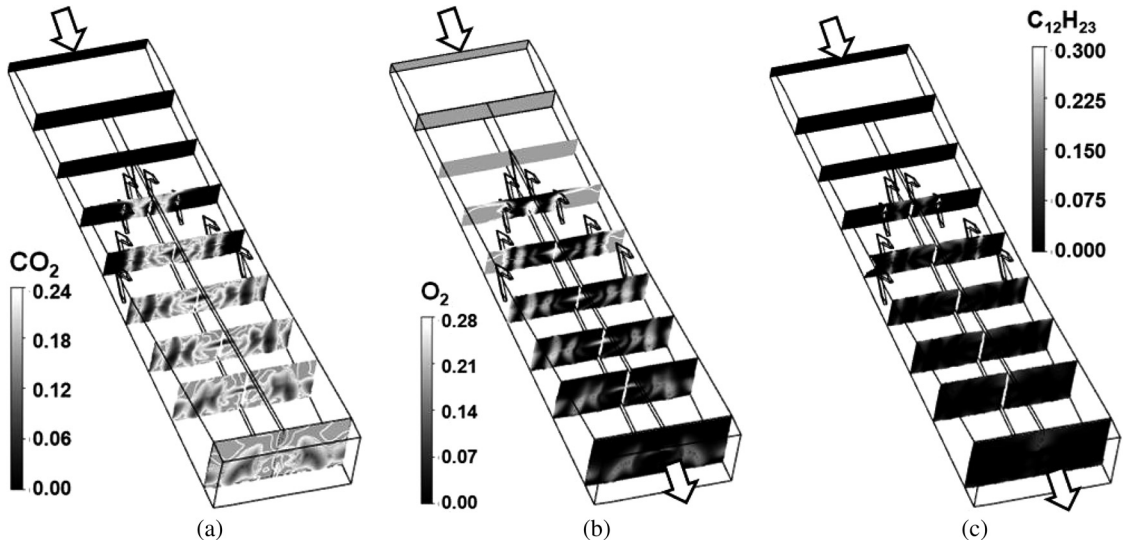

Fig. 8 Mass fraction distribution of (*a*) CO_2, (*b*) O_2, and (*c*) Jet-A ($C_{12}H_{23}$) vapor at various axial locations

burnt kerosene to the total amount of kerosene fuel injected in the combustor and found to be 78.2% for the present case. Thrust achieved from the combustor is calculated from the difference of the outlet momentum and inlet momentum of the combustor and is found to be 7350 N/kg s of fuel flow rate.

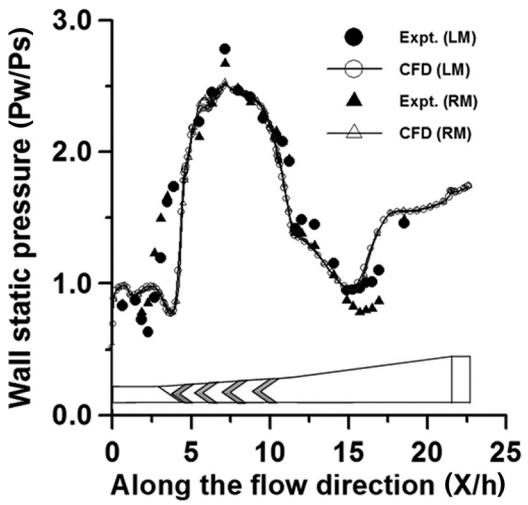

Fig. 9 Comparison of top wall pressure distribution ($Z = 1.6h$)

The comparison of the top wall pressures between the experiment and the CFD has been made in Fig. 9. Rise of wall static pressure due to the combustion has been found adjacent to the strut wall regions in both experiment and numerical simulation. Pressure distribution of both the modules in CFD looks almost similar. Eventhough overall comparison between the experiment and the CFD is fairly good, the peak pressure in the experiment seems to be slightly more compared to the CFD values. Also, the point of separation in experiment seems to be delayed in RM compared to CFD.

4.4.2 Effect of Mass Flow Rate of Vitiated Air. Mass flow rate of vitiated air was found to decrease with time during the experiment. To find out the effect of mass flow rate on top wall pressure and the performance of the combustor, two more simulations are carried out by changing the mass flow rate of the hot incoming air by 5% (case-2) and 10% (case-3). In the simulations, kerosene flow rate was kept the same. Comparison of top wall pressure distribution (RM) for these two cases along with baseline case is shown in Fig. 10. Overall, top wall pressures have been found to decrease with the decrease of mass flow rate. In the reaction intense zone ($X/h = 0.45$–0.8), the differences of the top wall pressure have been found more compared to the other axial locations. Combustion efficiency has been found to decrease (74.0% for case-2 and 70.9% for case-3) with the reduction of air flow rate. Similarly, thrust achieved from the combustor has been found to

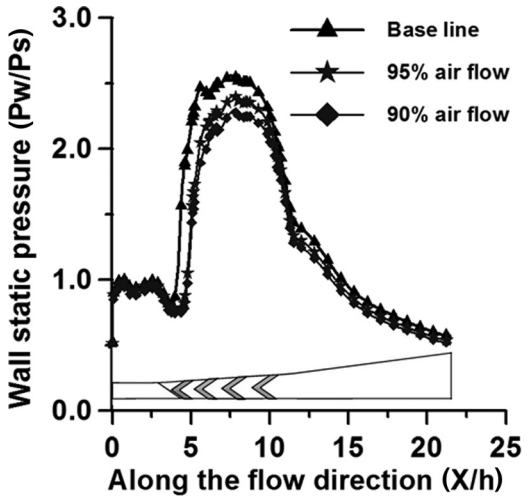

Fig. 10 Effects of vitiated air flow (RM)

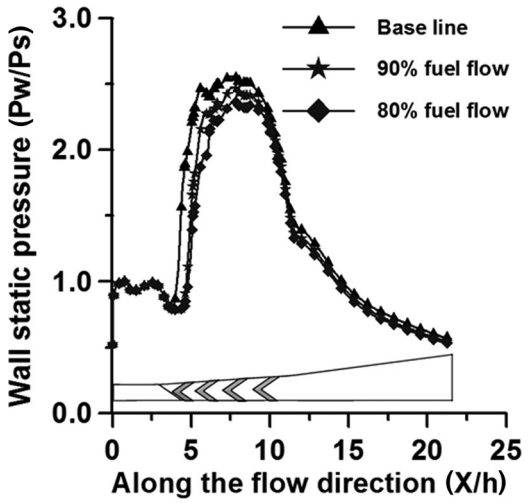

Fig. 11 Effects of fuel flow rate (RM)

be 6832 N/kg s and 6381 N/kg s fuel flow rate for case-2 and case-3, respectively, which accounts for a reduction of thrust by 7.1% and 13.2%, respectively, compared to the baseline combustor.

4.4.3 Effect of Fuel Flow Rate. During the test, some amount of leakage of kerosene was found from the combustor. To assess the effect of fuel flow rate, two more numerical simulations were carried out in the baseline configuration by reducing the fuel flow rate 10% (case-4) and 20% (case-5) in equal manner for all the struts. Comparison of top wall pressure distribution (RM) for these two cases along with baseline case is shown in Fig. 11. Top wall pressures have been found to decrease with the decrease of fuel flow rate. Upstream interaction has been found to decrease with lesser fuel flow rate. The differences of the top wall pressure have been found to be less in the downstream regions compared to the reaction intense zones. Combustion efficiency has been found to increase (80.5% for case-4 and 83.9% for case-5) with the reduction of fuel flow rate. Though overall thrust has been found to decrease by 5.3% and 10.5% for case-4 and case-5, respectively, compared to the baseline value, thrust per unit fuel flow rate has been increased by 5.4% and 12.0%, respectively, for case-4 and case-5 compared to baseline configuration. This is because of increase in combustion efficiency.

5 Conclusions

Post-test numerical simulations of full-scale eight struts-based scramjet combustor with facility nozzle are carried out for test inflow conditions. Both nonreacting and reacting flow simulation are carried out. Different simulations are performed to study the effect of mass flow and fuel flow rate on top wall pressure distribution and combustor performance. Three-dimensional RANS equations are solved along with k–ε turbulence model. Single-step chemical reaction with LPTM is used for combustion of kerosene fuel. Top wall pressures have been found to decrease with the decrease in mass flow rate. Fairly good match of the top wall pressure has been found both for nonreacting and reacting flow with the experimental results. In addition, to see the effect of fuel flow rate, two more simulations have been carried out by reducing the fuel flow rate by 10% and 20% equally from the struts. It has been observed that both the combustion efficiency and the thrust availability per unit fuel flow rate increase with the decrease of fuel flow rate.

Acknowledgment

The authors would like to acknowledge the constant support and encouragement provided by the Project Director, HSTDV and LPD Team, DOP, DRDL during the course of the work and for providing the experimental data.

Nomenclature

A_{ebu}, B_{ebu} = model coefficient of EDM
D = Rosin–Rammler particle diameter
EDM = eddy dissipation model
h = height of the combustor
k = turbulent kinetic energy
LM = left side module of the combustor
LPTM = Lagrangian particle tracking method
M = Mach number
P = pressure
R = right side module of the combustor
RANS = Reynolds-averaged Navier–Stokes
r_k = stoichiometric ratio
$R_{k,EDM}$ = mixing rate of EDM
T = temperature
X, Y, Z = three-axes direction
y = mass fraction

Greek Symbols

γ = measure of particle size distribution
ε = turbulent kinetic energy dissipation rate
ρ = density

Subscripts

f, ox, p = fuel, oxidizer, product
i, out = inlet, outlet
o = total condition of a flow
s = static

References

[1] Feri, A., 1964, "Review of Problems in Application of Supersonic Combustion," J. R. Aeronaut. Soc., **68**(645), pp. 575–597.
[2] Waltrup, P. J., 1987, "Liquid-Fueled Supersonic Combustion Ramjet: A Research Perspective," J. Propul. Power, **3**(6), pp. 515–524.
[3] Curran, E. T., 2001, "Scramjet Engines: The First Forty Years," J. Propul. Power, **17**(6), pp. 1138–1148.
[4] Edward, A. K., and Joseph, A. S., 1973, "Liquid Jet Injection Into a Supersonic Flow," AIAA J., **11**(9), pp. 123–1224.
[5] Li, J. G., Yu, G., Zhang, X. Y., and Huang, Q. S., 2000, "Combustion of Kerosene in a Supersonic Stream," AIAA Paper No. 2000–0615.
[6] Gruber, M. R., Donbar, J. M., Carter, C. D., and Hsu, K. Y., 2004, "Mixing and Combustion Studies Using Cavity-Based Flame Holders in a Supersonic Flow," J. Propul. Power, **20**(5), pp. 769–778.

[7] Yu, G., Li, J. G., Chang, X. Y., Chen, L. H., and Sung, C. J., 2003, "Fuel Injection and Flame Stabilization in Liquid–Kerosene Fueled Supersonic Combustor," J. Propul. Power, **19**(5), pp. 885–893.
[8] Miyajima, H., Chinzei, N., Mitani, T., Wakamatser, Y., and Maita, M., 1992, "Development Status of the NAL Scramjet Engine Test Facility and Subscale Scramjet Engine," AIAA Paper No. 92-5094.
[9] Sunami, T., Sakuranaka, N., Tani, K., Kiraiwa, T., and Shimura, T., 1997, "Mach 4 Test of a Scramjet Engine—Effect of Isolator," Proceedings of the 13th International Symposium of Air Breathing Engine, AIAA, Washington, DC, pp. 615–625.
[10] Dufour, E., and Bouchez, M., 2001, "Computational Analysis of a Kerosene Fueled Scramjet," AIAA Paper No. 2001–1817.
[11] Bouchez, M., Dufour, E., and Montazel, X., 1998, "Hydrocarbon Fueled Scramjet for Hypersonic Vehicles," AIAA Paper No. 1998–1589.
[12] Montgomery, C. J., Zhao, W., Tam, C. J., Eklund, D. R., and Chen, J. Y., 2004, "CFD Simulations of a 3-D Scramjet Flameholder Using Reduced Chemical Kinetic Mechanisms," AIAA Paper No. 2004-3874.
[13] Manna, P., Behera, R., and Chakraborty, D., 2008, "Liquid Fueled Strut Based Scramjet Combustor Design—A Computational Fluid Dynamics Approach," J. Propul. Power, **24**(2), pp. 274–281.
[14] Pannerselvam, S., Thiagarajan, V., Ganesh, A. T. K., Geetha, J. J., Ramanujachari, V., and Prahlada, 2005, "Airframe Integrated Scramjet Design and Performance Analysis," Paper No. 2005-1280.
[15] ANSYS CFX, 2007, *Release, 11.0: Installation and Overview*, ANSYS, Canonsburg, PA.
[16] Saha, S., and Chakraborty, D., 2006, "Reacting Flow Computation of Staged Supersonic Combustor With Strut Injection," AIAA Paper No. 2006-3895.
[17] Javed, A., and Chakraborty, D., 2006, "Numerical Simulation of Supersonic Combustion of Pylon Injected Hydrogen Fuel in Scramjet Combustor," J. Inst. Eng., **87**, pp. 1–6.
[18] Manna, P., Behera, R., and Chakraborty, D., 2007, "Thermochemical Exploration of a Cavity Based Supersonic Combustor With Liquid Kerosene Fuel," J. Aerosp. Sci. Technol., **59**(4), pp. 246–258.
[19] Behera, R., and Chakraborty, D., 2006, "Numerical Simulation of Kerosene Fueled Ramp Cavity Based Scramjet Combustor," J. Aerosp. Sci. Technol., **58**(2), pp. 104–112.
[20] Marquardt Corporation, 1964, "Supersonic Combustion Tests in an 8000 FPS Air Stream," Van Nuys, Los Angeles, CA, Report No. 6064.
[21] ANSYS ICEM-CFD, 2007, *Release, 11.0: Installation and Overview*, ANSYS, Canonsburg, PA.